

# STELLAR COLLAPSE AND GRAVITATIONAL WAVES

Chris L. Fryer

*Theoretical Astrophysics, Los Alamos National Laboratories, Los Alamos, NM, 87545*

Daniel E. Holz and Scott A. Hughes

*Kavli Institute for Theoretical Physics, UC Santa Barbara, Santa Barbara, CA 93106*

Michael S. Warren

*Theoretical Astrophysics, Los Alamos National Laboratories, Los Alamos, NM, 87545*

## Abstract

The new generation of gravitational wave (GW) detectors have the potential to open a novel window onto the violent dynamics of core collapse. Although it is certain that core collapse events generate gravitational radiation, understanding the characteristics of the radiation — whether it can be measured with these detectors, and the best way to go about doing so — is a challenging problem. In this chapter we review the promise of GWs as observational probes, including a discussion of the current state of GW detectors, and discuss the status of work to understand the waves generated by stellar core collapse.

## 1. Introduction

For quite some time the collapse of massive stellar cores in supernova explosions has been regarded as likely to be an interesting and important source of gravitational radiation (see, for example, Eardley 1983 for an early review of the subject). Core collapse events certainly produce GWs: large amounts of mass ( $\sim 1\text{--}100 M_{\odot}$ ) flow in a compact region ( $\sim 10^8\text{--}10^9$  cm) at relativistic velocities ( $v/c \sim 1/5$ ). These characteristics are *necessary* conditions for a source to be an interesting GW source; however, they are *not* sufficient conditions. Detailed analysis is needed to understand whether these potentially interesting sources are in fact

sufficiently asymmetric to be strong radiators, and whether we can understand their robust features well enough to search for them with GW observatories.

Theoretical modeling of stellar collapse has become increasingly sophisticated in recent years: collapse theorists can now model collapses in three dimensions (albeit requiring enormous amounts of CPU time), and can include important physics such as neutrino transport and the equation of state of very dense matter. Previously, most estimates of GW emission from stellar collapse were (of necessity) rather idealized, typically studying the evolution of instabilities in rotating fluid distributions (Chandrasekhar 1969, Centrella et al. 2000, New et al. 2000). Although extremely valuable in establishing the conditions under which strongly radiating instabilities can occur, these analyses do not incorporate important physical effects which occur during stellar collapse. Using modern collapse models, estimates of GW emission can now be constructed that more realistically reflect the phenomenology of stellar collapse. Coupling these modern models with the wisdom that has been gleaned from decades of study from the idealized cases, we should now be able to assemble a robust picture of the GWs arising from core collapse.

The maturity of modern collapse simulations is quite timely: they arrive just as broad-band GW detectors based on laser interferometry are coming into existence. Science runs with the initial generations of these detectors have just begun, although these instruments have not yet reached their design sensitivities. Furthermore, the design sensitivities are not really at the level where stellar core collapse can be considered a realistically interesting signal (Fryer, Holz, & Hughes 2002, hereafter FHH). However, the detectors' sensitivities have improved quite rapidly<sup>1</sup>, and a vigorous R&D program promises to push the sensitivities to better levels very rapidly (Gustafson, Shoemaker, Strain, & Weiss 1999). The possibility of seeing core collapse GWs is stronger than ever<sup>2</sup>.

In this chapter we review the state of our present knowledge of GW events. We first present an overview of GW physics, focusing on the properties of the waves themselves and how one detects them, plus a brief review of the current state of the various GW interferometers. (We note that the discussion of the detectors' state is quite likely to be out of date by the time this article appears in print.) This material is largely

---

<sup>1</sup>The LIGO detectors have improved their sensitivities by several orders of magnitude across a wide frequency band in the first nine months of 2002.

<sup>2</sup>It's worth noting that there is always a chance—albeit a small one—that a relatively nearby star could go supernova and produce an anomalously strong signal. The current configuration of LIGO would likely have seen SN 1987a, were it to have been operating back then. The last thing that the GW detection community wants is to miss another such event!

taken from a recent review article (Hughes et al. 2001) with some updating to reflect the current status of the detectors. We then turn to an in-depth discussion of GWs from core collapse events, comparing the likely properties of these waves to the detection thresholds of the new interferometric detectors. This discussion is based to a large extent on the review of FHH, with some updating based on recent work on r-modes and 3-D simulations.

## 2. GWs and detectors: overview

Gravitational radiation is a natural consequence of general relativity, first described more-or-less correctly by Albert Einstein (1918). GWs are tensor perturbations to the metric of spacetime, propagating at the speed of light, with two independent polarizations. As electromagnetic radiation is generated by the acceleration of charges, gravitational radiation arises from the acceleration of masses. Electromagnetic waves are created (at lowest order) by the time changing charge dipole moment, and are thus dipole waves. Monopole EM radiation would violate charge conservation. At lowest order, GWs come from the time changing quadrupolar distribution of mass and energy; monopole GWs would violate mass-energy conservation, and dipole waves violate momentum conservation.

GWs act tidally, stretching and squeezing objects as they pass through. Because the waves arise from quadrupolar oscillations, they are themselves quadrupolar in character, squeezing along one axis while stretching along the other. When the size of the object that the wave acts upon is small compared to the wavelength (which is the case for all ground-based detectors), forces arising from the two GW polarizations act as in Fig. 1. The polarizations are named “+” (plus) and “×” (cross), as a result of the orientation of the axes associated with their force lines.

Interferometric GW detectors measure this tidal field via their action upon a widely-separated set of test masses, arranged as in Fig. 2. Each mass is suspended with a sophisticated pendular isolation system to eliminate the effect of local ground noise. Above the resonant frequency of the pendulum (typically of order 1 Hz), the mass moves freely. In the absence of a GW, the sides  $L_1$  and  $L_2$  shown in Fig. 2 are taken to have the same length,  $L$ .

Suppose the interferometer in Fig. 2 is arranged so that its arms lie along the  $x$  and  $y$  axes of Fig. 1. Suppose further that a wave impinges on the detector down the  $z$  axis, and the “+” polarization axes are aligned with the detector’s arms. The tidal force of this wave stretches one arm while squeezing the other; each arm oscillates between stretch

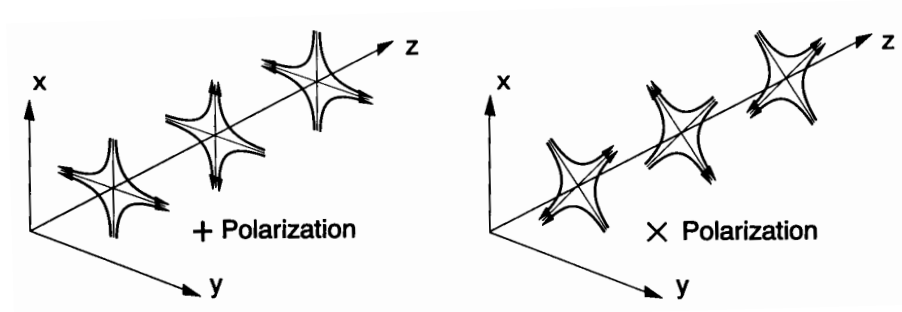


Figure 1. The lines of force associated with the two polarizations of a GW (from Abramovici et al. 1992).

and squeeze as the wave itself oscillates. The wave is detectable by measuring the separation of the test masses in each arm. In particular, since one arm is always stretched while the other is squeezed, we can monitor the length difference of the two arms:

$$\delta L(t) \equiv L_1(t) - L_2(t) . \quad (1)$$

For the case discussed above, this change in length turns out to be the armlength times the + polarization amplitude:

$$\delta L(t) = h_+(t)L . \quad (2)$$

The GW acts as a dimensionless strain in the detector;  $h$  is often referred to as the “wavetrain”. Equation (2) is derived by applying the equation of geodesic deviation to the separation of the test masses, using a GW tensor on a flat background spacetime to develop the curvature tensor; see Thorne (1987), Sec. 9.2.2 for details. We obviously do not expect astrophysical GW sources to align themselves in as convenient a manner as described above. Generally, both polarizations of the wave influence the test masses:

$$\frac{\delta L(t)}{L} = F^+ h_+(t) + F^\times h_\times(t) \equiv h(t) . \quad (3)$$

The antenna response functions  $F^+$  and  $F^\times$  weight the two polarizations in a quadrupolar manner as a function of a source’s position and orientation relative to the detector; see Thorne (1987), Eqs. (104a,b) and associated text.

The test masses at the ends of each arm are made of a highly transparent material (fused silica in present designs; perhaps sapphire in future

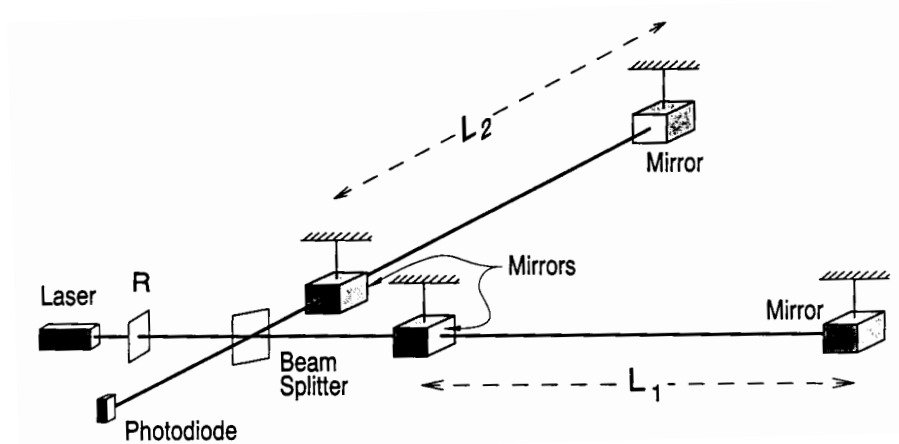


Figure 2. Layout of an interferometer for detecting GWs (from Abramovici et al. 1992).

upgrades). All of the test masses are faced with dielectric coatings such that they are extremely good reflectors of the 1.064 micron infrared laser light. The mirrors at the far end of each arm have amplitude reflectivities approaching unity. The mirrors at the corner joining the arms are less reflective, since they must couple the light into the Fabry-Perot cavity arms. The corner mirrors' multilayer dielectric coatings have power reflectivities  $T \sim 3\%$ . A very stable laser beam is divided at the beam-splitter, directing light into the two arm cavities. If the finesse of the cavity is  $\mathcal{F}$  and the amplitude reflectivity of the corner mirrors is  $r_{\text{corner}}$ , then each photon makes on average  $\mathcal{F}/\pi \simeq \sqrt{r_{\text{corner}}}/(1 - r_{\text{corner}}) \sim 65$  bounces. The light from the two arms then recombines at the beam-splitter. The mirrors are positioned so that, in the absence of a GW, all of the light goes back to the laser and the photodiode reads no signal. If a signal is present, the relative phase  $\Phi$  of the two beams must have changed by an amount proportional to  $h$ , changing the light's interference pattern. With no intervention, this would cause light to leak into the photodiode. In principle, the wavetrain  $h$  could be read from the intensity of this light. In practice, a system of servo loops controls the system such that destructive interference is guaranteed — the photodiode is kept dark, and is thus called the “dark port”. The wavetrain  $h$  is encoded in the servo signals used to keep the dark port dark.

The energy flux carried by GWs scales with  $\dot{h}^2$  (where the overdot represents a time derivative). To conserve energy flowing through large

spheres, the wavetrain falls off with distance as  $1/r$ . We have already argued that the lowest order contribution to the waves is due to the changing quadrupole moment of the source. To order of magnitude, this moment is given by  $Q \sim (\text{source mass})(\text{source size})^2$ . Since the wavetrain is dimensionless, the scaling must take the form

$$h \sim \frac{G \ddot{Q}}{c^4 r}. \quad (4)$$

The second time derivative of the quadrupole moment is given approximately by  $\ddot{Q} \simeq 2Mv^2 \simeq 4E_{\text{kin}}^{\text{ns}}$ , where  $v$  is the source's internal velocity, and  $E_{\text{kin}}^{\text{ns}}$  is the nonspherical part of its internal kinetic energy. Strong sources of gravitational radiation are sources that have strong non-spherical dynamics; hence, core collapse events must be quite asymmetric in order to give off considerable energy in GWs.

For an interesting rate of observable events, detectors must be sensitive to sources at rather large distances. For example, to detect several stellar collapse event in a year, our detectors must reach  $r \sim 10$  Mpc. For stellar collapse, a reasonable estimate of the non-spherical kinetic energy is  $E_{\text{kin}}^{\text{ns}}/c^2 \sim 0.1 M_{\odot}$ . Plugging these numbers into Eq. (4) yields the estimate

$$h \sim 10^{-21} - 10^{-22}. \quad (5)$$

These tiny numbers set the sensitivity required to measure GWs. Combining this scale with Eq. (3) says that for every kilometer of baseline  $L$ , we must measure a distance shift between the arm lengths,  $\delta L$ , of better than  $10^{-16}$  centimeters.

The prospect of achieving such stringent displacement sensitivities often strikes people as insane. How can light, whose wavelength  $\lambda \sim 10^{-4}$  cm is  $10^{12}$  times larger than the typical displacement, be used to measure that displacement? For that matter, how is it possible that thermal motions don't wash out these tiny effects?

That such measurement is possible with laser interferometry was first analyzed thoroughly by Weiss (1972).<sup>3</sup> We examine first how a 1 micron laser can measure a  $10^{-16}$  cm effect. As mentioned above, the light bounces back and forth roughly 100 times before leaving the arm cavity (corresponding to about half a cycle of a 100 Hz GW). The light's accumulated phase shift during those 100 round trips is

$$\Delta\Phi_{\text{GW}} \sim 100 \times 2 \times \Delta L \times 2\pi/\lambda \sim 10^{-9}. \quad (6)$$

---

<sup>3</sup>It should be noted that the possibility of detecting GWs with laser interferometers has an even longer history, reaching back to Pirani in 1956, and was independently proposed by several workers: Gertsenshtein and Pustovoit in 1962, Weber in the 1960s, and Weiss c. 1970. See Sec. 9.5.3 of Thorne (1987) for further discussion and references.

This phase shift is measurable provided that the shot noise at the photodiode,  $\Delta\Phi_{\text{shot}} \sim 1/\sqrt{N}$ , is less than  $\Delta\Phi_{\text{GW}}$ .  $N$  is the number of photons accumulated over the measurement;  $1/\sqrt{N}$  is the magnitude of phase fluctuation in a coherent state, appropriate for describing a laser. We therefore must accumulate  $10^{18}$  photons over the roughly 0.01 second measurement, which translates to a laser power of about 100 watts. In fact, as was pointed out by Drever (1983), one can use a much less powerful laser: even in the presence of a GW, only a tiny portion of the light that comes out of the interferometer’s arms goes to the photodiode. The vast majority of the light is sent back to the laser. An appropriately placed mirror bounces this light back into the arms, *recycling* it. The recycling mirror is shown in Fig. 2, labeled “R”. With that mirror, a laser of  $\sim 10$  watts drives several hundred watts to circulate in the “recycling cavity” (the optical cavity between the recycling mirror and the arms), and  $\sim 10$  kilowatts to circulate in the arms.

Thermal excitations are overcome by averaging over many many vibrations. For example, the atoms on the surface of the interferometers’ test mass mirrors oscillate with an amplitude

$$\delta l_{\text{atom}} = \sqrt{\frac{kT}{m\omega^2}} \sim 10^{-10} \text{ cm} \quad (7)$$

at room temperature  $T$ , with  $m$  the atomic mass, and with a vibrational frequency  $\omega \sim 10^{14} \text{ s}^{-1}$ . This amplitude is huge relative to the effect of the GW—why doesn’t it wash out the wave? GWs are detectable because the atomic vibrations are random and incoherent. The  $\sim 7$  cm wide laser beam averages over about  $10^{17}$  atoms and at least  $10^{11}$  vibrations in a typical measurement. These atomic vibrations cancel out, becoming irrelevant compared to the coherent effect of a GW. Other thermal vibrations, however, end up dominating the detectors’ noise spectra in certain frequency bands. For example, the test masses’ normal modes are thermally excited. The typical frequency of these modes is  $\omega \sim 10^5 \text{ s}^{-1}$ , and they have mass  $m \sim 10 \text{ kg}$ , so  $\delta l_{\text{mass}} \sim 10^{-14} \text{ cm}$ . This, again, is much larger than the effect we wish to observe. However, the modes are very high frequency, and so can be averaged away provided the test mass is made from material with a very high quality factor  $Q$  (so that the mode’s energy is confined to a very narrow band near  $\omega$ , and thus doesn’t leak into the band we want to use for measurements). Understanding the physical nature of noise in GW detectors is an active field of current research; see Levin (1998), Liu & Thorne (2000), Santamore & Levin (2001), Buonanno & Chen (2001a,b), Hughes & Thorne (1998), Creighton (2000), and references therein for a glimpse of recent work. In all cases, the fundamental fact to keep in mind is that a GW

acts *coherently*, whereas noise acts *incoherently*, and thus can be beaten down provided one is able to average away the incoherent noise sources.

## 2.1 Current detectors

The first generation of long baseline, kilometer-scale interferometric GW detectors are in operation or are being constructed and commissioned at several sites around the world. Briefly, the major ground-based interferometric GW projects are as follows:

- **LIGO.** Three LIGO (Laser Interferometer Gravitational-wave Observatory) interferometers are currently operating: two in Hanford, Washington (with 2 and 4 km arms, sharing the same vacuum system), and one in Livingston, Louisiana (4 km arms). An aerial view of the Hanford site is included in Fig. 3. The LIGO detectors are designed to operate as power recycled Michelson interferometers with arms acting as Fabry-Perot cavities. The large distance between sites (about 3000 km) and differing arm lengths are designed to support coincidence analysis. Much current research and development is focused on advanced LIGO detector design. The goal of these planned improvements is to provide a broader frequency band and a  $\sim 10$ -fold increase in range for sources via a lowered noise floor.
- **Virgo.** Virgo, the Italian/French long baseline GW detector, is under construction near Pisa, Italy (Marion 2000). It has 3 km arms and advanced passive seismic isolation systems. In most respects, Virgo is similar to LIGO; a major difference is that it should achieve better low frequency sensitivity in its first generation due to its advanced seismic isolation. Virgo will usefully complement the LIGO detectors, strengthening coincidence analysis and significantly improving source position determination.
- **GEO600.** GEO600 is a 600 meter interferometer constructed by a British-German collaboration near Hannover, Germany (Lück et al. 2000). It uses advanced interferometry and advanced low noise multiple pendulum suspensions, serving as a testbed for advanced detector technology, and allowing it to achieve sensitivities comparable to the multi-kilometer instruments.
- **TAMA300.** The TAMA detector near Tokyo, Japan can already claim significant observation time, with more than 1000 hours of operation (Ando et al. 2001). It has achieved a peak strain sensitivity of  $h \sim 3 \times 10^{-19} \text{ Hz}^{-1/2}$  at frequencies near 1000 Hz. TAMA



has 300 meter arms and is operated in the recombined Michelson configuration with Fabry-Perot arms. A much improved 3 km detector is currently under design (Kuroda et al. 2000).

- **ACIGA.** The Australian Consortium for Interferometric Gravitational Astronomy plans to build an observatory near Perth, Australia (McClelland et al. 2000). They are presently engaged in the construction of an 80 meter research interferometer, which can be extended to kilometer scale. They are studying advanced detection methods and technologies which could lead to much decreased noise floors in advanced interferometers.

Since interferometric GW detectors have nearly equal sensitivity in all directions, it is essentially impossible to deduce pointing information from the output of a single detector. To get accurate information about the source direction it is necessary to make use of time-of-flight differences between detectors. To do this the detectors must be widely spaced, and cannot be collinear. At the very minimum, three sites are needed for acceptable pointing. A fourth detector, widely removed from the plane of the other three, is particularly valuable for improving directional information. Thus a detector in Australia would greatly add to the science output of the GW observatory network, which is otherwise confined entirely to the northern hemisphere.

LIGO is representative of the design and operation principles of these interferometers, so we shall focus on it for the remainder of our discussion.

## 2.2 LIGO overview

Construction of both LIGO facilities and vacuum systems was completed in early 2000. Both observatories have mostly concentrated to date on detector commissioning and a series of “Engineering Runs”, leading to the first “Science Run”, which began in August 2002. This will be followed by more frequent and longer Science Runs until 2006/7, when major detector upgrades are scheduled. In parallel with the commissioning effort and Engineering/Science Runs, the LIGO collaboration is also focused on the research and development of advanced detectors, promising a wider detector band and greatly improved sensitivity.

The LIGO detectors operate as power recycled Michelson interferometers with Fabry-Perot arms; see Fig. 3. Very high duty cycle is needed for each interferometer in order to effectively use the full network for coincidence analysis, which is necessary for achieving a low false detection rate and high confidence observations. The wide (3000 km) separation

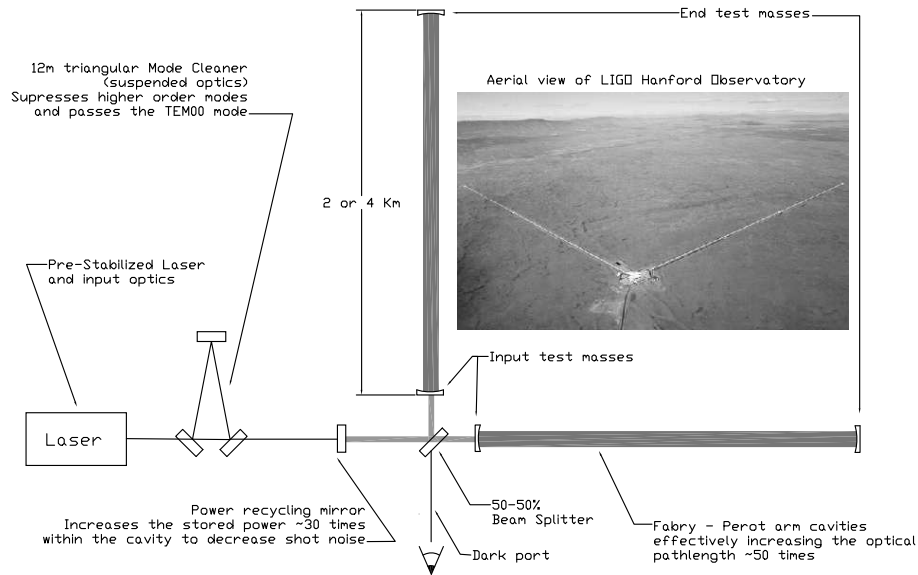


*Figure 3.* Simplified optical layout of a LIGO interferometer. Shown here are the prestabilized laser, the input mode cleaner, the recycling mirror, and the test mass mirrors. As discussed in Sec. 2, servo loops ensure that the recombined light destructively interferes so that the dark port is kept dark. The GW signal is read out from the forces needed to keep the recombined light in destructive interference.

between the LIGO sites is large enough that the chance of environmentally induced coincidence events is small. Both sites are equipped with environmental sensors that cover a wide range of possible disturbances that otherwise could cause false detections. For example, LIGO monitors the local seismic background, electromagnetic fluctuations, acoustic noise, cosmic radiation, dust, vacuum status, weather, power line transients, and magnetic fields (using ultra-sensitive magnetometers at several locations at each observatory).

We now briefly describe the operating principles of LIGO, the major sources of noise that limit sensitivity, and plans for future upgrades.

**Laser, optics, and configuration.** The basic optical layout of the LIGO detectors is shown in Figure 3. LIGO uses a Nd:YAG near infrared laser (wavelength 1064 nm) with peak power  $\sim 10\text{W}$  as the light source. Various electro-optical components and servo loops are used to stabilize both the frequency and power of the laser.

The light from the pre-stabilized laser passes through the input optics and is coupled into the 12 meter, triangular mode cleaner cavity. The

mode cleaner passes only the TEM<sub>00</sub> mode, eliminating higher order modes. Starting with the mode cleaner, every major optical component is within a large vacuum system, operating at  $10^{-9}$  Torr. After conditioning by the mode cleaner, the light enters the interferometer. All major optics in the interferometer are suspended on a single steel wire loop, mechanically isolated from the ground by vibration isolators and controlled by multiple servo loops. The mirrors are made of fused silica with extremely high mechanical  $Q$  and polished to within  $\sim 1$  nanometer RMS. They have high homogeneity, low bulk loss, and multi-layer coatings with less than 50 ppm scattering loss. Each mirror is actuated by four precision coils, each positioned around a permanent magnet glued to the back side of the test masses. The coil assembly also features a sensitive shadow sensor for local control. Additional optical levers and wavefront sensors provide more precise sensing. The laser beam is coupled into the arms by a beam splitter. Each arm is a Fabry-Perot optical cavity, increasing the effective length of the arm to magnify the phase shift (proportional to cavity finesse) caused by the wave. The stored power within the interferometer is built up by the partially transmitting recycling mirror.

An operating interferometer tries to keep the dark port perfectly dark, adjusting the positions of the various optical components such that light coming out of the arms destructively interferes and no light goes to the photodetector. When this is achieved, the interferometer is on *resonance*, with maximum power circulating in the arms. Several interconnected control loops are used to achieve and then maintain resonance. An interferometer on resonance is usually described as *locked*. Keeping lock must be highly automated, requiring minimal operator interaction for high uptime. The GW signal is extracted from the servo signals used to maintain the lock and correct for the changing length difference between the arms.

**Noise sources.** The sensitivity of GW interferometers is limited by a large number of noise sources. We list here some of the most important and interesting fundamental noise sources; many of these were originally recognized, and had their magnitudes estimated, by Weiss (1972).

- **Seismic noise.** Ambient seismic waves (e.g., loading of the continental shelf by surf striking the coast) or culturally induced seismic waves (e.g., passing trucks, logging, cattle guards) continuously pass under the test masses of the detector. The natural motion of the surface peaks around 150 mHz; this is called the “micro-seismic peak”. Cultural noises tend to be at higher frequencies, near several Hz. The test masses must be carefully isolated from

the ground to effectively mitigate seismic noise. Seismic noise will limit the low frequency sensitivity of first generation ground-based GW detectors; the only way to get good performance below  $\sim 1$  Hz is to put one's detector space. This is a major motivator for the LISA<sup>4</sup> gravitational-wave detector.

- **Thermal noise.** Thermally excited vibrational modes of the test mass or the suspension system will couple with the resonances of the system. By improving the  $Q$  of the components one can isolate the thermally induced noise to the resonant frequency.
- **Shot noise.** The number of photons in the input laser beam fluctuates; this surfaces as noise at the dark port. This noise is proportional to  $1/\sqrt{\text{recycling gain} \times \text{input laser power}}$ . Increasing the recycling gain and/or increasing the laser power lowers the shot noise. Unfortunately, high power in the cavities induces other unwanted effects, such as radiation pressure noise (discussed in the next item) or thermal lensing (local deformation of the optical surfaces of the cavity). The right choice of laser power and recycling gain involves a compromise among many sources of noise.
- **Radiation pressure noise.** Fluctuations in the number of photons reflecting from the mirrors induces a fluctuating force on the mirrors. This effect scales as  $\sqrt{\text{recycling gain} \times \text{input laser power}}$ —the inverse of the proportionality entering the shot noise: there is a penalty to increasing the laser power. Reducing shot noise and radiation pressure noise in tandem is a topic of advanced detector R&D; see Buonanno & Chen (2001a,b) and references therein for further discussion.
- **Gravity gradient noise.** When seismic waves, atmospheric pressure fluctuations, cars, animals, tumbleweeds, etc., pass near a GW detector, they act as density perturbations on the neighboring region. This in turn can produce significant fluctuating gravitational forces on the interferometer's test masses (Hughes & Thorne 1998; Creighton 2000), which is expected to become the limiting noise source at low frequencies for advanced ground-based detectors with high quality seismic isolation systems.
- **Laser intensity and frequency noise.** All lasers have some inherent noise, which causes fluctuations in both the laser's intensity and frequency. This noise does not cancel out perfectly when the

---

<sup>4</sup>The Laser Interferometer Space Antenna (Danzmann et al. 1998; Bender 2001).

signal from the two arms destructively recombines, and so some noise leaks into the dark port.

- **Scattered light.** Some laser light can scatter out of the main beam, and then be scattered back, coupling into the interferometer's signal. This light will carry information about its scattering surface, and will generally be out of phase with the beam, contaminating the desired signal. A dense baffling system has been installed to greatly reduce this source of noise.
- **Residual gas.** Any vacuum system contains some trace amount of gas that is extremely difficult to reduce; in LIGO, these traces (mostly hydrogen) are at roughly  $10^{-9}$  Torr. Density fluctuations from these traces in the beam path will induce index of refraction fluctuations in the arms. Residual gas particles bouncing off the mirrors can also increase the displacement noise.
- **Beam jitter.** Jitter in the optics will cause the beam position and angle to fluctuate slightly, causing noise at the dark port.
- **Electric fields.** Fluctuations in the electric field around the test masses can couple into the interferometric signal via interaction between the field and the induced or parasitic surface charge on the mirror surface.
- **Magnetic fields.** Fluctuations in the local magnetic field can affect the test masses when interacting with the actuator magnets bonded to the surface of the mirrors.
- **Cosmic showers.** High energy penetrating muons can be stopped by the test masses and induce a random transient due to recoil.

The initial LIGO detectors will be limited by seismic noise at low frequencies ( $\lesssim 50$  Hz), by thermal noise in the test mass suspensions at intermediate frequencies ( $\sim 50$ – $200$  Hz), and by shot noise at high frequencies ( $\gtrsim 200$  Hz). Present detector noise is above the target level, particularly at low and intermediate frequencies, though there has been much progress recently in approaching the target noise curve.

**Detector upgrades.** Much research within the experimental GW community focuses on developing technologies for improving the sensitivity of LIGO and other ground-based detectors. The first stage detectors are somewhat conservatively designed, ensuring that they can be operated without the excessive introduction of new technology. The price for this conservatism is limited astrophysical reach: current LIGO

sensitivity is such that detection of sources is plausible, but not particularly probable, based on our current understanding of sources.

To broaden the astrophysical reach of these instruments, major upgrades are planned for 2006/7. The goal of these upgrades is to push the lower frequency “wall” to lower frequencies, and push the noise level down by a factor  $\sim 10$  across the band. This will increase the distance to which sources can be detected by a factor of 10 – 15, and the volume of the universe which LIGO samples by a factor of 1000–3000. This will dramatically boost any measured event rates.

Discussion of these plans is given in Gustafson et al. (1999). Major changes include a redesigned seismic isolation system (pushing the wall down to about 10 Hz), a more powerful laser (pushing the shot noise down by about a factor of 10), and replacement of the optical and suspension components with improved materials to reduce the impact of thermal noise. In addition, the system will allow “tunable” noise curves—experimenters will be able to shape the noise curve to “chase” particularly interesting sources.

### 3. GW emission mechanisms

Several distinct physical mechanisms could drive GW emission in stellar core collapse. Following our earlier discussion (cf. Sec. 2 of FHH), we begin with a quick overview of GW generation; further detail and references can be found in Thorne (1987). We then discuss numerical methods of calculating wavestrains given a distribution of masses and mass currents, and the GWs produced by certain instabilities—bar modes, fragmentations, and r-modes.

Unlike FHH, we do *not* discuss the ringing of newly born black holes. A black hole that is distorted from its stationary Kerr configuration will radiate GWs that drive it back to the stationary state. A black hole formed in core collapse will certainly be distorted; if large amounts of material accrete onto it, it will be continually driven into new states of distortion. This in principle could form an interesting GW source. In practice, however, FHH show that it is not likely to be interesting as a LIGO source: the waves are emitted at high frequencies where detector sensitivities are poor, and the associated strain is unlikely to be interestingly large. The interested reader should consult FHH for further details.

#### 3.1 Formal overview

The conventional approach to calculating the GW emission of a given mass distribution is via a multipole expansion of the perturbation  $h_{\mu\nu}$  to

a background spacetime  $g_{\mu\nu}^B$ . The transverse-traceless projection of this metric, evaluated in the radiation zone, is the metric of the radiation field. The lowest (quadrupole) order piece of this field is (Thorne 1980)

$$h_{jk}^{\text{TT}} = \frac{1}{d} \left[ 2 \frac{G}{c^4} \frac{d^2}{dt^2} \mathcal{I}_{jk}(t-r) + \frac{8}{3} \frac{G}{c^5} \epsilon_{pq(j} \frac{d^2}{dt^2} \mathcal{S}_{k)p}(t-r) n_q \right]^{\text{TT}}. \quad (8)$$

$\mathcal{I}_{jk}$  and  $\mathcal{S}_{jk}$  are the mass and current quadrupole moments of the source,  $d$  is the distance from the source to the point of measurement,  $\epsilon_{ijk}$  is the antisymmetric tensor, and  $n_q$  is the unit vector pointing in the propagation direction. Parentheses in the subscripts indicate symmetrization over the enclosed indices, and the superscript TT indicates that one is to take the transverse-traceless projection. Most GW estimates are based on Eq. (8). When bulk mass motions dominate a source's dynamics, the first term describes the radiation that is generated; for example, it produces the well-known "chirp" associated with binary inspiral. The second term dominates for a system whose dynamics are dominated by mass currents, as is the case for radiation from the r-mode instability.

When the background spacetime is flat (or nearly so) the mass and current moments have particularly simple forms. For example, in Cartesian coordinates the mass quadrupole is given by

$$\mathcal{I}_{jk} = \int d^3x \rho \left[ x^j x^k - \frac{1}{3} r^2 \delta_{jk} \right], \quad (9)$$

where  $\rho$  is the mass density, and  $\delta_{jk} = 1$  for  $j = k$  and 0 otherwise. The  $\delta_{jk}$  term ensures that the resulting tensor is trace free.

GWs carry energy and angular momentum from the source (Isaacson 1968). The lowest order contribution to the power,  $P$ , emitted in GWs is due to variations in the quadrupole moment:

$$P = \frac{dE}{dt} = \frac{1}{5} \frac{c^5}{G} \left\langle \frac{d^3 \mathcal{I}_{jk}}{dt^3} \frac{d^3 \mathcal{I}_{jk}}{dt^3} \right\rangle. \quad (10)$$

Although radiated power is useful for understanding the effect of GW emission on a source's dynamical evolution,  $P$  is not useful for detectability estimates. Instead, one needs an estimate of the waveltrain  $h$ , which is directly measured by the detectors. When averaged over all source orientations and sky positions, the power and strain are related by

$$P = \frac{\pi^2 c^3}{G} f^2 d^2 \overline{h^2}, \quad (11)$$

where  $f$  is the GW frequency and  $d$  is the luminosity distance to the source. For a given strain, higher frequency waves radiate more energy. Because of detector noise, however, higher frequency waves are not necessarily more detectable.

### 3.2 Bar modes

Bar modes are an instability in which the material in the stellar core forms a rapidly rotating bar-like structure. Such a structure has a rapidly varying quadrupole moment, and as such is potentially a copious emitter of GWs. Bar mode instabilities occur in objects whose rotational kinetic energy exceeds some fraction of their potential energy, with the ratio generally written as  $\beta \equiv T/|W|$ . Standard lore (Chandrasekhar 1969) tells us that an object is unstable on a secular time scale if  $\beta \gtrsim 0.14$ , and is dynamically unstable if  $\beta \gtrsim 0.27$ . This lore may be violated if the density profile is not centrally peaked: if centrifugal forces produce a peak in the density off the source’s rotational center, dynamical instabilities can set in at much lower values of  $\beta$  (Centrella et al. 2000). Most core-collapse simulations with up-to-date progenitor models, however, find that the mass distribution does not suffer a centrifugal hang-up. This follows from the fact that, in these modern progenitor models, the rotation speeds of the collapsing stellar cores is relatively small (Heger 1998), particularly when compared to earlier models (Rampp, Müller, & Ruffert 1998). In these simulations, the density is centrally concentrated, and thus the low critical values of Centrella et al. (2000) do not apply. Nonetheless, the rotational energy of these models can be quite large (cf. Fig. 4), so  $\beta$  is likely to be large enough that bar-mode instabilities will occur.

Heartened by this possibility, we review here expressions for bar mode GW emission. Consider a bar of mass  $m$  and length  $2r$ , rotating with angular frequency  $\omega$ . The GW energy radiated is given, in the quadrupole approximation, by

$$P_{\text{bar}} = \frac{32}{45} \frac{G}{c^5} m^2 r^4 \omega^6. \quad (12)$$

A detector at a distance  $d$  from the source would measure an rms strain

$$h_{\text{bar}} = \sqrt{\frac{32}{45} \frac{G}{c^4} \frac{m r^2 \omega^2}{d}}. \quad (13)$$

Note that, due to symmetry, the frequency of the emitted GWs is twice the bar’s rotation frequency.

### 3.3 Fragmentation instability

To set a physically motivated upper limit to the GW emission that might be produced in stellar collapse, imagine that the collapse material fragments into clumps, which then orbit for some number of cycles as the collapse proceeds. For concreteness, consider the material fragmenting into a binary system (though it could very well fragment into more objects). Such a matter distribution is plausible if the density distribution



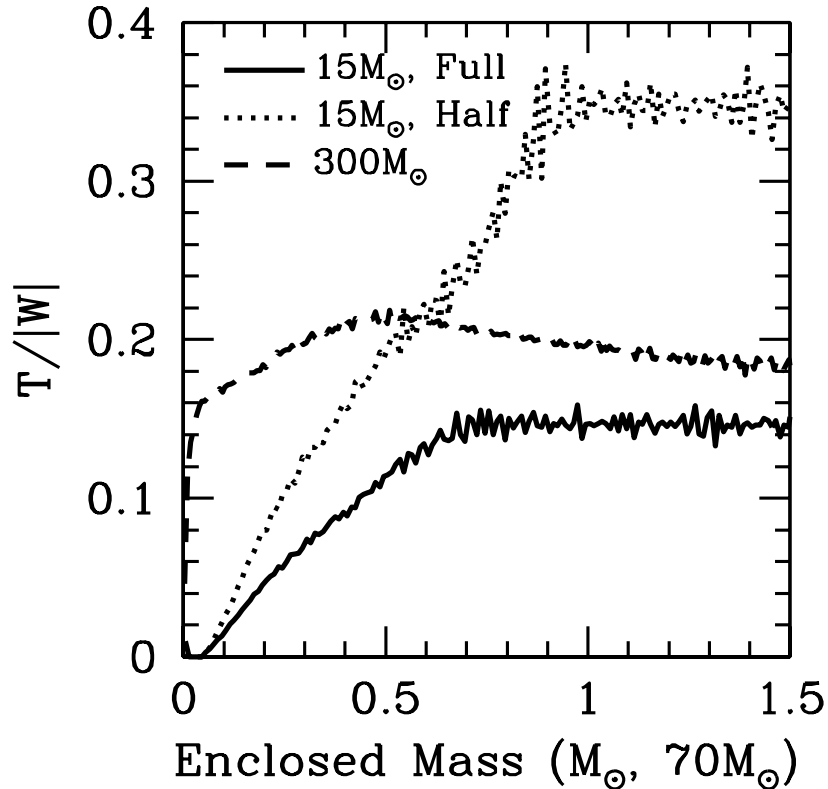


*Figure 4.* Rotational energy divided by gravitational energy ( $\beta \equiv T/|W|$ ) vs. mass for collapsing stars. The horizontal axis is in solar masses for the  $15 M_{\odot}$  stellar models, in fractions of  $70 M_{\odot}$  for the  $300 M_{\odot}$  models. Shown are rotating core collapse (full rotation), 1.6 seconds after bounce; core collapse with half rotation, 1.4 seconds after bounce; and direct collapse of a  $300 M_{\odot}$  star, 1.9 seconds after bounce. Note that  $T/|W|$  for the half rotating progenitor is actually larger than for the fully rotating progenitor. This is because that star is more compact.

during collapse peaks off center, as is indicated by some simulations of collapsing Population III stars (Fryer, Woosley, & Heger 2001).

Two bodies, each of mass  $m$ , in circular orbit about one another at a frequency  $\omega$  and with separation  $2r$ , radiate GWs with power and mean

strain

$$P_{\text{bin}} = \frac{128}{5} \frac{G}{c^5} m^2 r^4 \omega^6 \quad (14)$$

$$h_{\text{bin}} = \sqrt{\frac{128}{5} \frac{G}{c^4} \frac{m r^2 \omega^2}{d}}. \quad (15)$$

These formulae make no assumption about orbital frequency, and thus apply to, for example, pressure supported as well as Keplerian orbits. For Keplerian orbits,  $4\omega^2 r^3 = Gm$ , so the above expressions become

$$P_{\text{bin}} = \frac{2}{5} \frac{G^4}{c^5} \frac{m^5}{r^5} \quad (16)$$

$$h_{\text{bin}} = \sqrt{\frac{8}{5} \frac{G^2}{c^4} \frac{m^2}{r d}}. \quad (17)$$

Note that if the “horizons” of the two bodies touch ( $r = 2mG/c^2$ ), the power radiated reaches a maximum of  $P = c^5/80G \sim 10^{57}$  ergs  $\text{s}^{-1}$ , independent of the system’s mass. The length of time such emission can be sustained scales with the total mass—supermassive black hole binaries do radiate more than microscopic ones.

### 3.4 R-modes

R-modes are peculiar instabilities that may occur in neutron stars. These modes are large scale oscillations in the *current* distribution of the fluid—they drive very little change in the star’s density, and as such, their GW generation is described using the second term of Eq. (8). R-modes have been of particular interest to GW studies (e.g., Lindblom, Owen, & Morsink 1998; Andersson, Kokkotas, & Schutz 1999; Owen et al. 1998) because they are unstable to GW emission: gravitational radiation tends to *increase* the amplitude of the mode. Lindblom, Owen, & Morsink (1998) first mapped out the range of stellar spin and temperature for which the viscosity was unlikely to damp away this runaway growth, and concluded that many hot, young neutron stars were likely to be important sources of GWs. Current thinking is that the r-modes of young hot neutron stars are actually unlikely to be important sources of GWs. Most analyses assume that the growth of the mode will eventually be limited by nonlinear hydrodynamic effects. Arras et al. (2002) find, after a careful analysis of mode-mode coupling effects, that the saturation amplitude of the modes is far smaller—by four orders of magnitude—than had been assumed previously. Their rather forceful conclusion is that r-modes are completely undetectable.

In FHH we examined the r-mode waves that could be produced by various collapse scenarios that lead to neutron star formation. Our con-

clusions were broadly in line with those of Owen et al. (1998). In fact, we reinforced those conclusions somewhat by pointing out that material falling back onto the newly-born neutron star could spin it up and reawaken an r-mode instability that had previously decayed away. Re-examining the conclusions in light of the wisdom of Arras et al. (2002), we are forced to a rather different outcome—the r-mode waves are unlikely to ever be detected.

As a consequence of this new understanding, we will end our r-modes discussion here. Interested readers can re-examine Sec. 2.4 of FHH, noting that the amplitude factor  $\alpha$  should be around  $10^{-5}$ – $10^{-4}$ , rather than the 0.1–1 considered there. With this in mind, the results for r-modes from young remnants of stellar collapse (Secs. 3.2.2 and 4.2.2 of FHH) are *much* more pessimistic as far as direct detection is concerned.

### 3.5 Direct numerical calculation

If one has a computational model of a core-collapse scenario, one can calculate the GW emission predicted by that model by numerically applying Eq. (8) to the mass and current distributions predicted by that model. Naive implementation of Eq. (8) works poorly: computing the required derivatives numerically (by evaluating the quadrupole moments on multiple time slices and differencing), introduces spurious numerical noise. However, if the potentials which drive the motion of the matter are known, the time derivatives can be rewritten as spatial derivatives, and the GW emission can be calculated using data from a single time slice. Calculations demonstrating this technique are given in Finn & Evans (1990), Blanchet, Damour, & Evans (1990), and Centrella & McMillan (1993). The Centrella & McMillan paper is specialized to smooth particle hydrodynamics (SPH).

Fryer & Warren (2002) have recently modeled core collapse with a 3-dimensional code using SPH. One of the goals of this work will be to test whether the instabilities discussed above, particularly bar modes and fragmentation, actually occur in a computational stellar collapse model. At present, the only GWs produced by these models come from the large scale, convective motions of matter near the protoneutron star (cf. Fig. 5). The GWs from these motions are computed using the formulae given in Centrella & McMillan (1993). We discuss these results at length below.

The work of Fryer & Warren (2002) coupled an equation of state for dense matter and a flux-limited diffusion neutrino transport scheme into a parallel 3-dimensional SPH code. This code includes all of the physics used in 2-dimensional models less than a decade ago (e.g. Herant et al.

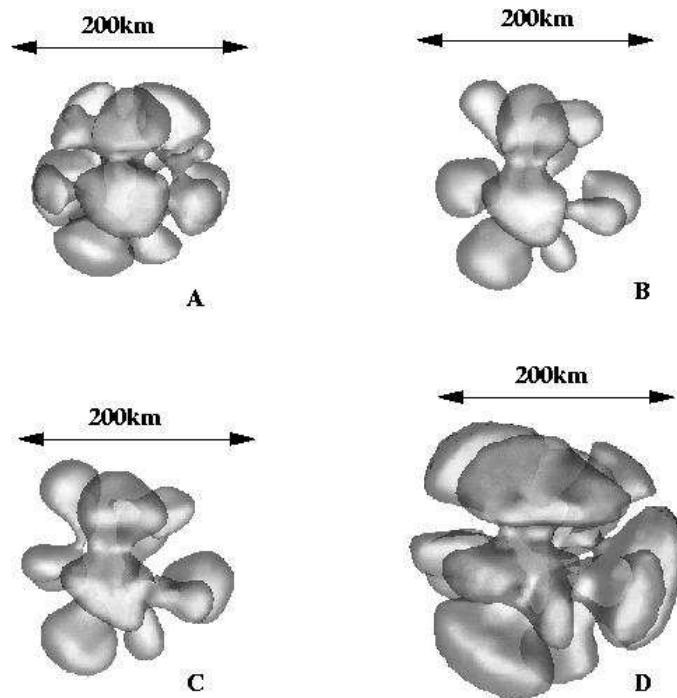


*Figure 5.* Isosurfaces of upward moving bubbles (radial velocities moving outward at 1000 km/sec) as a function of time ( $t_A < t_B < t_C < t_D$ ) from the 3-dimensional simulations of Fryer & Warren (2002). Note that the number of modes decreases slightly as the flows merge over time (compare panel A with later panels).

1994) and shows the remarkable progress in simulations of core-collapse. Fig. 5 shows the convective upwells of the first such 3-dimensional simulations of the collapse of a symmetric star. These simulations assumed spherically symmetric implementation of gravity for better comparison with past 2-dimensional work. However, the code developed by Fryer & Warren (2002) has a tree-based algorithm for calculating gravity and can be used to model the collapse of rotating or asymmetric cores. The first rotating models are running and, as predicted by the 2-dimensional simulations (Fryer & Heger 2000), show convection that is primarily limited to the polar regions (Fig. 6).

Improvements still must be made: a more sophisticated neutrino algorithm is needed to accurately model neutrino heating, general relativistic and equation of state effects also contribute to uncertainties. However, progress along all these fronts is being made.

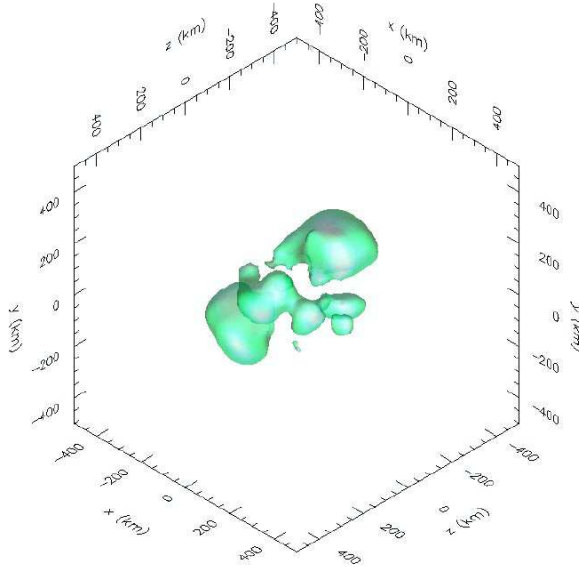


*Figure 6.* Isosurfaces of upward moving bubbles (radial velocities moving outward at 1000 km/sec) from the rotating 3-dimensional simulations of Fryer & Warren (2003). Due to the angular momentum gradient, which prevents convection along the equator, most of the convection occurs along the rotation ( $z$ ) axis.

#### 4. Results for GW emission

Applying the various mechanisms discussed in the previous section, we now estimate GW strengths for two important stellar collapse scenarios—supernovae, and the death of Population III stars. In each case, we discuss what is known about the rates of these events and their likely angular momentum distribution (both of which strongly impact their importance as GW sources), and then estimate their GW strengths. In both cases, we sketch the wavestrains likely for waves arising from bar mode instabilities, and a possible fragmentation instability, comparing these waves to the noise level that is the goal of the second generation LIGO-II detectors (in particular, the broad-band configuration of those detectors; cf. Gustafson, Shoemaker, Strain, & Weiss 1999). For supernovae, we also discuss the recent results of Fryer & Warren (2002), for gravitational waves generated in a 3-D numerical calculation of convective motions in a supernova explosion.

## 4.1 Supernovae

**Formation rate and angular momentum.** The supernova rate is fairly well known, lying somewhere between 1 per 50–140 years in the Galaxy (Cappellaro et al. 1997). It is not clear, however, what fraction of these core-collapse events (if any) are rotating rapidly enough to develop these instabilities, and thereby emit detectable GWs.

Insight into the angular momentum distribution can be gained by studying pulsars, the compact remnants of core-collapse supernovae. From measurements of young pulsars, we know that at least some neutron stars are born with periods faster than 20 ms. Whether or not any neutron stars are born with millisecond periods is harder to ascertain—pulsars spin down as they emit radiation, and the spindown rate is not particularly well determined. A recent analysis of Chernoff & Cordes (private communication) found that the initial spin periods could be fit with a Gaussian distribution peaking at 7 ms, with sub-ms pulsars lying beyond the 2-sigma tail. Does this mean that less than 10% of pulsars are born spinning with millisecond periods, or does it mean that many pulsars are born spinning rapidly, and GW emission removes a considerable amount of their angular momentum? It is to be noted that the analysis of Chernoff & Cordes is very sensitive to their choice of spindown rates and other uncertainties in their population study; they stress that such results should be taken with a great deal of caution. Though such large and important uncertainties complicate efforts to estimate the likely magnitudes of GW emission following supernovae, they also illustrate the impact that GW observations could have. Even a solid null result (no GWs seen from core-collapse with a high degree of confidence) would have important impact, telling us that rapidly rotating newly born neutron stars are very rare.

Stellar theorists have now produced models of core-collapse progenitors which include angular momentum (Heger 1998). Though these simulations build in a number of assumptions about the angular momentum transport in the massive star, they provide some handle on the angular momentum distribution in the collapsing core. We base our analysis on the angular momentum profiles from the core-collapse simulations of  $15 M_{\odot}$  stars by Fryer & Heger (2000), which use these latest progenitors and model the core-collapse through supernova explosion (Models 1,5; cf. Fig. 2 of FHH).

**GWs from bar modes and fragmentation.** Because the angular momentum distributions used by Fryer & Heger (2000) have peak values significantly lower than those used in the past, there is no centrifugal

hang-up. The collapse proceeds nearly identically to a non-rotating star, with a density distribution peaked at the center of the star. This makes it harder for bar-mode instabilities to develop, and produces weaker GW emission. During bounce, the neutron star is not compact enough to quickly drive bar-mode instabilities.

However, the explosion produced by these rotating core-collapse supernovae is much stronger along the poles than along the equator (Fryer & Heger 2000), causing much of the low angular-momentum material to be ejected. Hence, after the explosion— $\sim 1$  s after collapse— $\beta$  can increase to high enough values that bar-mode instabilities are likely to develop (cf. Fig. 4). The amount of matter enclosed by the proto-neutron star extends in all cases beyond  $\sim 1 M_{\odot}$ , corresponding to values of  $\beta$  which are certainly above the secular instability limit ( $\beta \sim 0.14$ ), and probably also above the dynamic instability limit ( $\beta \sim 0.27$ ). Notice in Fig. 4 that  $\beta$  is actually larger for the model which has less initial angular momentum. This is because this model has contracted more, and is spinning more rapidly. Notice that we have to push to these conditions merely to produce bar-mode instabilities. It is even less likely that fragmentation will occur in core-collapse supernovae.

The Fryer & Heger (2000) simulations are axisymmetric (2D) and so, by construction, cannot produce a bar mode instability. However, we can get a handle on the *potential* of these models to radiate by a bar mode instability by taking the mass and angular momentum distributions of the Fryer & Heger models and imagining that some fraction of the mass in these models participates in such an instability. We do this by assuming that all of the matter up to some enclosed mass becomes unstable and forms a bar (conserving angular momentum), and then calculate the GW emission as a function of total unstable mass. One should bear in mind that we assume *all* of the enclosed mass ends up in the bar. These estimates are thus relatively strong upper limits (although the strain could increase if we allowed the bar to contract and spin up). We illustrate the detectability of waves from this bar model in Figure 7. Each point on this plot illustrates a different possible bar, varying the amount of mass that participates in the instability. Open circles illustrate the wavetrain for a single GW cycle; filled circles give the characteristic strain obtainable if the bar radiates coherently for 100 cycles. This plot demonstrates that bar modes are potentially promising sources of waves if bars remain coherent for at least a moderate ( $\sim 50$ – $100$ ) number of GW cycles.

Since the density is centrally peaked, a fragmentation instability is unlikely to occur in core-collapse supernovae. However, if it did occur,

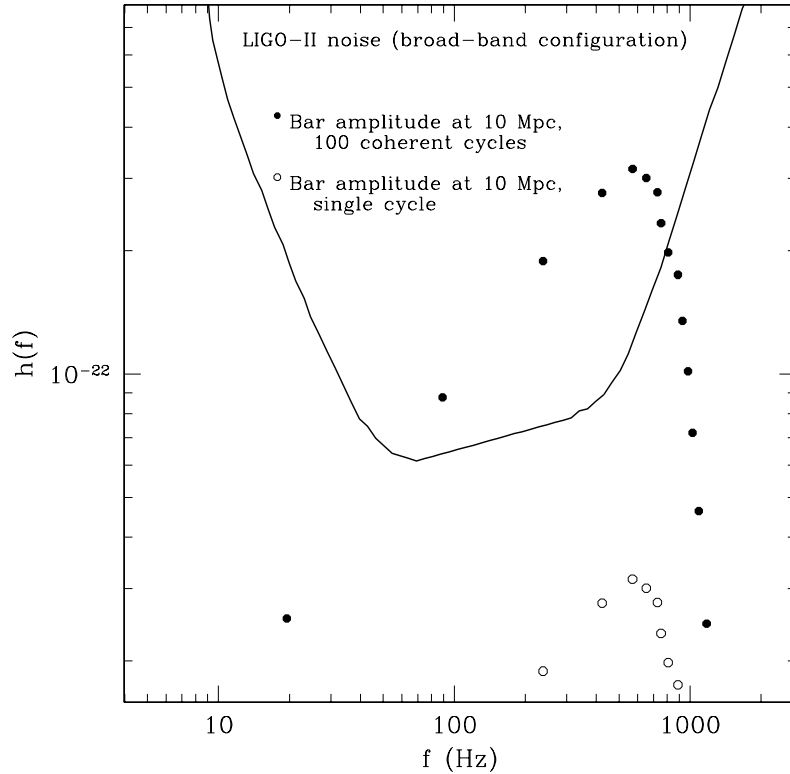


*Figure 7.* Bar mode gravitational waves compared to broad-band LIGO-II noise. We use the Fryer & Heger (2000) models for core collapse, and then estimate GW emission as follows: we assume that all mass inside a given radius participates in a bar mode instability and forms a bar, conserving angular momentum as it does so. Each point represents the waves produced by a particular choice of radius, moving to larger radii from right to left. An open circle is the strain from a single wave cycle of the bar; a closed circle is the integrated strain that would be measured if the bar were to remain coherent for 100 GW cycles. The range between the open and closed circles suggests that bar-mode waves could be of interesting strength provided that they remain coherent for a minimum of  $\sim 50$ –100 cycles.

even the single-cycle strain would be quite large ( $\sim 10^{-22}$ ), and fall in an interesting band (from a few hundred Hz up to a kilohertz or so).

**Numerically calculated GW estimates.** As computational models improve we can expect to reach the point where a 3-dimensional numerical calculation can adequately model an asymmetric supernova explosion, and diagnose whether the various instabilities discussed above



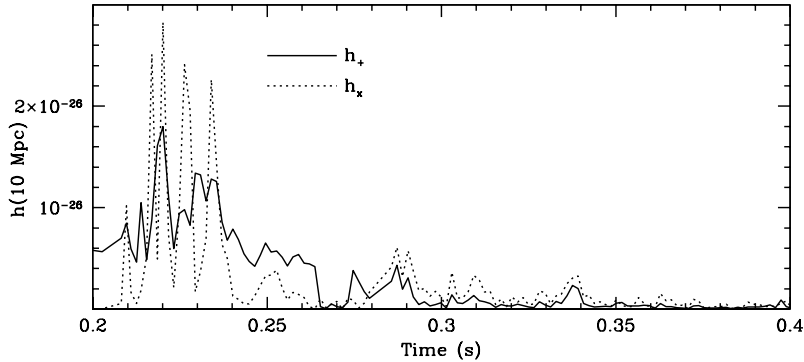


Figure 8. Magnitude of the wavetrain for convective motions in a non-rotating 3-D stellar collapse model (cf. Fig. 5), for a supernova at 10 Mpc.

are likely to actually occur. We're not quite there yet, but recent progress has been impressive. As our physical understanding of supernovae improves, and as more powerful computational resources become available, we can look forward to serious numerical studies that model realistic supernova explosions.

At present the most relevant models that can be studied to estimate GW emission in a 3-D calculation are those produced by Fryer & Warren (2002). The only dynamical aspect of this model with sufficient asymmetry to produce GWs are the convective cells bubbling through the stellar core (cf. Fig. 5; the models are currently non rotating). The GW strengths in these bubbles is simply estimated by postprocessing the model's data using the formulae of Centrella & McMillan (1993). The magnitude of the GW strain expected from this model's convective behavior is shown in Fig. 8 for an explosion at 10 Mpc.

The first rotating simulations are now being run (Fryer & Warren 2003), but with the rotation speeds expected from stellar evolution models (Heger 1998), it does not appear that bar-mode instabilities develop both because of the low, but realistic angular momentum in the Heger models and because the convection and viscosity (dominated by numerical viscosity) transport out this angular momentum. If bar-modes do not develop, the dominant gravitational wave signal occurs at bounce where models by Dimmelmeier, Font, & Müller (2002a,2002b) are among the most physically accurate.

These convective GWs are extremely weak—even though they arise from the rapid overturning motions of dense matter in the star, the multipolar distribution of this matter is not ideally distributed to be a

strong source of GWs. Even in a galactic explosion (distance to source  $\sim 10$  kpc), these waves would be weak ( $h \sim 10^{-23}$ ). Preliminary results from rotating simulations from Fryer & Warren (2003) also do not develop strong bar modes and hence do not have strong GW signals (only a  $\sim 2$  order of magnitude increase). Even higher angular momenta are required to cause fragmentation. If the results of Fryer & Warren (2003) are correct, fragmentation can be ruled out in core-collapse supernovae. Future 3-D models will study the effects of angular momentum transport and will also include the effects of asymmetries in collapse to find the maximum gravitational wave signals that may develop from core-collapse supernovae.

## 4.2 Collapse of very massive stars

At solar metallicity, stellar winds severely limit the pre-collapse mass of massive stars—very few massive stars will remain massive up to the time of collapse. As these winds are driven by the opacity of metals in the stellar envelope, it is likely that mass loss from winds will decrease as the fraction of metals in the envelope is reduced. Population III stars are the first generation of stars formed in the early universe, before stars formed the metals that abound today. Here we review the death of very massive (100–500  $M_{\odot}$ ) Population III stars. Like Chandrasekhar-massed white dwarfs, these stars must suffer one of two fates: either they explode in a giant thermonuclear explosion (“hypernova”), or they collapse to form black holes. The fate is determined by the stellar mass. If the star’s mass exceeds  $\sim 260 M_{\odot}$ , it will collapse to a black hole (Fryer, Woosley, & Heger 2001; Baraffe, Heger, & Woosley 2001). However, if the star is rotating, rotational (plus thermal) support prevents the star from undergoing immediate collapse to a black hole (Fryer, Woosley, & Heger 2001). Rotating, very massive stars collapse and bounce, forming a much larger compact core than those produced by core-collapse supernovae: a 50–70  $M_{\odot}$ , 1000–2000 km proto-black hole instead of the 1  $M_{\odot}$ , 100 km proto-neutron star. This rotating proto-black hole is susceptible to bar instabilities and may produce a strong GW signal (see also Madau & Rees 2001).

**Formation rate and angular momentum.** Estimating the rate of core-collapse for very massive stars depends on two rather uncertain quantities: the amount of matter found in Population III stars, and the number of these stars which actually collapse to form black holes. The mass distribution of stars at birth is known as the initial mass function (IMF). Today the IMF is peaked toward low mass stars, such

that 90% of stellar core-collapse occurs in stars between 8 and  $\sim 20 M_{\odot}$ , and only 1% of core-collapse occurs in stars more massive than  $40 M_{\odot}$ . However, it has long been believed that the first generation of stars after the Big Bang tended to be more massive than stars formed today (e.g., Silk 1983; Carr & Rees 1984). Recent simulations by Abel, Bryan, & Norman (2000) suggest that the typical mass of first generation stars is  $\sim 100 M_{\odot}$ , and it is possible that a majority of Population III stars had masses in excess of  $100 M_{\odot}$ .

The light from these very massive stars re-ionizes the early universe; from this we can derive a constraint on the formation rate of these stars. Although we expect that their photons ionized a significant fraction of the early universe, there should not be so many stars that they ionize the universe several times over. Using our best estimates of the re-ionization fraction, the amount of ultraviolet photons produced by these massive stars, and the ionization efficiency of massive stars, one finds that 0.01%–1% of the baryonic matter in the universe was incorporated into very massive stars (Abel, Bryan, & Norman 2000). This corresponds to about  $10^4$ – $10^7$  very massive stars produced in a  $10^{11} M_{\odot}$  galaxy, or a rate of massive stellar collapse as high as one every few thousand years.

We should temper these optimistic statements with two caveats. First, these are Population III stars, and so are born at high redshift ( $z \gtrsim 5$ ). As they evolve to collapse in less than a few million years (Baraffe, Heger, & Woosley 2001), they will only be observed near to the high redshifts of their birth. In addition, although we may believe our formation rate of very massive stars (within a few orders of magnitude), it is currently impossible to determine what fraction of very massive stars are produced with masses beyond the  $\sim 260 M_{\odot}$  mass limit necessary for black hole formation. The Galaxy could produce a million of these objects, or perhaps just a few hundred. Assuming 1–10 million very massive stars per galaxy beyond  $z = 5$  gives us a secure upper limit.

The rotation of these stars has again been calculated using the stellar evolution code developed by Heger (1998); for this analysis we use the Fryer et al. (2001) rotation profiles.

**GWs from bar modes and fragmentation.** We expect the proto-black hole formed in the collapse of a massive star to become secularly unstable (Fig. 4), and these secular instabilities are likely to develop before the proto-black hole collapses to a black hole (Fryer, Woosley, & Heger 2001). Given the large amount of mass ( $\sim 70 M_{\odot}$ ) and angular momentum these objects possess, it is not surprising that these objects can produce strong GW signals. However, the cosmological redshift moves the peak of the source waves out of the band of LIGO detectors:

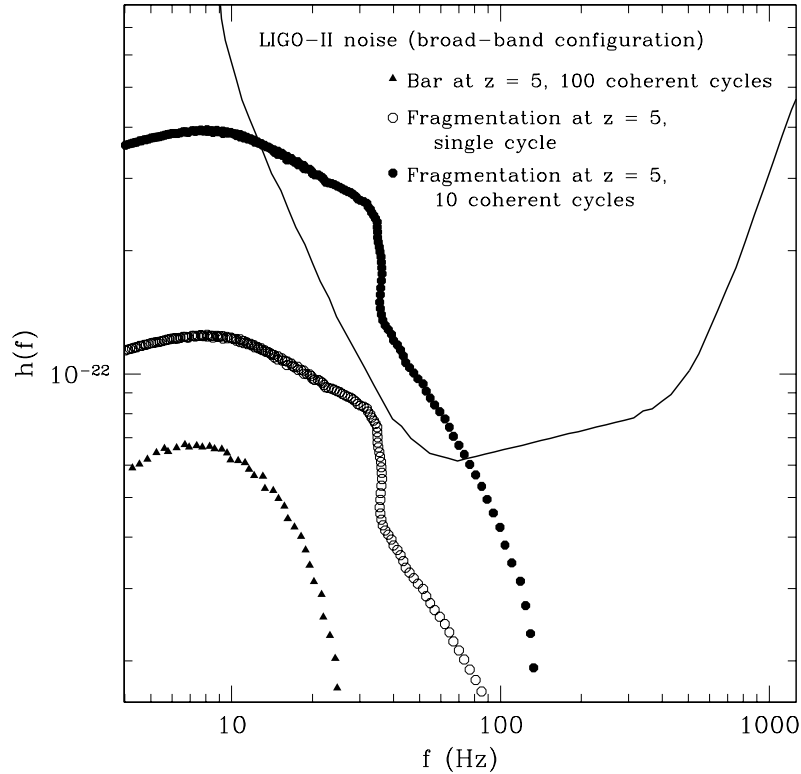


*Figure 9.* Possible bar mode and fragmentation instability GW signals for collapse of  $300 M_{\odot}$  Population III star. As in Fig. 7, each point corresponds to all mass inside a particular radius participating in the instability, conserving angular momentum. The prospects for detecting bar modes from these collapse events are extremely bad: the cosmological redshift pushes this signal far out of the LIGO band. Waves generated by a fragmentation instability are potentially interesting: both their strains and frequencies are significantly higher, and might be accessible to LIGO, particularly if the signal remains coherent for some number of cycles.

even at the relatively low value  $z = 5$  (corresponding to a luminosity distance  $\sim 48$  Gpc in the currently popular “concordance cosmology” [Wang, Tegmark, & Zaldarriaga 2002]), the strain from bar modes peaks at frequencies less than 10 Hz, with a strain  $8 \times 10^{-23}$ . This is well below the LIGO II threshold. Even coherent integration over  $\sim 100$  cycles is unlikely to produce a detectable signal; see Fig. 9.

The waves from massive star collapse may be detectable, however, if a fragmentation instability occurs. With our crude model of fragmentation, we find that both strain and frequency are boosted if the core

splits into two pieces which then fall into a Keplerian orbit, conserving angular momentum. If this instability occurs and the pieces orbit coherently for  $\sim 10$  cycles, these waves may be detectable at redshifts  $z \sim 5$ ; see Figure 9.

## 5. Summary & concluding thoughts

One clear conclusion can be drawn from this survey: despite the impressive recent progress in our understanding of core collapse, we *still* have a relatively poor grasp of the processes that drive GW emission in these events. Past work on instabilities, when coupled with 2-D models of stellar collapse, provide a decent estimate of the range of wave strengths and frequencies that are possible, but do not provide specifics for what is to be expected from collapse.

Progress and future understanding will only come as these models are further generalized, building in the rotation or core oscillations that seem needed (Fryer & Heger 2000) to explain asymmetries in supernovae (Wang et al. 2001). Fully 3-D simulations, such as those from Fryer & Warren 2002, hold great promise for extending our knowledge of the collapse process. Better stellar models, better neutrino transport algorithms and the inclusion of general relativistic effects will allow modelers to unambiguously extract the effects of GWs. If the GW detector sensitivities continue to dramatically improve, one can hope that GW data will meaningfully impact core-collapse work later in the decade. As noted in Sec. 4.1, even a solid null result would provide useful information. An unambiguous *non*-null result (perhaps in coordination with other astronomical instruments) would be most exciting of all, and may open our clearest window onto the processes occurring deep inside collapsing stellar cores.

## Acknowledgments

We thank Peter Bender, Craig Hogan, and Szabolcs Marká for allowing us to use material from Hughes et al. (2001), and we thank Kip Thorne for permission to reproduce Figs. 1 and 2. The 3-D simulations were funded by a *Scientific Discovery through Advanced Computing* grant, and were performed on the IBM SP at the National Energy Research Scientific Computing Center. The work of DEH and SAH is supported at the KITP by NSF Grant PHY-9907949.

## References

- Abel, T., Bryan, G. L., Norman, M. L. 2000, ApJ, 540, 39.  
 Abramovici, A. et al. 1992, Science, 256, 325

- Ando, M. et al. 2001, *Phys. Rev. Lett.* 86, 3950.
- Andersson, N., Kokkotas, K., & Schutz, B. F. 1999, *ApJ*, 510, 846.
- Arras, P., Flanagan, E. E., Morsink, S. M., Schenk, A. K., Teukolsky, S. A., and Wasserman, I. 2002, *ApJ*, submitted; astro-ph/0202345.
- Baraffe, I., Heger, A., & Woosley, S. E. 2001, *ApJ*, 550, 890.
- Bender, P.L. 2001, in *Gravitational Waves*, eds. I. Ciufolini, V. Gorini, V. Moschella, and P. Fre, (Institute of Physics Publishing, Bristol, UK), p.115.
- Blanchet, L., Damour, T., & Schäffer, G. 1990, *MNRAS*, 242, 289.
- Buonanno, A. & Chen, Y. 2001, *Phys. Rev. D*, 64, 042006.
- Buonanno, A. & Chen, Y. 2001, *Class. Quantum Grav.* 18, L95.
- Cappellaro, E., Turatto, M., Tsvetkov, D. Tu., Bartunov, O. S., Pollas, C., Evans, R., & Hamuy, M. 1997, *A&A*, 322, 431.
- Carr, B. J. & Rees, M. J. 1984, *MNRAS*, 206, 315.
- Centrella, J. M., New, K. C. B., Lowe, L. L., & Brown, J. D. 2000, *ApJ*, 550, 193.
- Chandrasekhar, S. 1969, *Ellipsoidal Figures of Equilibrium* (New Haven: Yale University Press).
- Creighton, T. 2000, *Phys. Rev. D*, submitted; gr-qc/0007050.
- Danzmann, K. et al. 1998, *LISA Pre-Phase A Report*, 2nd Edition (Report MPQ-233, Max-Planck Institut für Quantenoptik, Garching, Germany), p. 1
- Dimmelmeier, H., Font, J., & Müller, E. 2002, *A&A*, 388, 917
- Dimmelmeier, H., Font, J., & Müller, E. 2002, *A&A*, 393, 523
- Drever, R. W. P. 1983, in *Gravitational Radiation*, eds. N. Deruelle and T. Piran (North Holland: Amsterdam), p. 321.
- Eardley, D. M. 1983, in *Gravitational Radiation*, eds. N. Deruelle and T. Piran (North Holland: Amsterdam), p. 257.
- Einstein, A. 1918, *Königlich Preußische Akademie der Wissenschaften Berlin, Sitzungsberichte*, p. 154.
- Finn, L. S. & Evans, C. 1990, *ApJ*, 351, 588.
- Fryer, C. L. & Heger, A. 2000, *ApJ*, 541, 1033.
- Fryer, C. L., Holz, D. E., & Hughes, S. A. 2002, *ApJ*, 565, 430; referred to in the text as FHH.
- Fryer, C. L. & Warren, M. S. 2002, *ApJ*, 574, L65.
- Fryer, C. L. & Warren, M. S. 2003, in preparation
- Fryer, C. L., Woosley, S. E., & Heger, A. 2001, *ApJ*, 550, 372.
- Gustafson, E., Shoemaker, D., Strain, K., & Weiss, R. 1999, *LSC White Paper on Detector Research and Development*, LIGO Document T990080-00-D.
- Heger, A. 1998, Ph.D. thesis, Technische Univ. München.
- Hughes, S. A., Marká, S., Bender, P. L., & Hogan, C. J. 2001, to appear in the *Proceedings of the 2001 Snowmass Meeting*; astro-ph/0110349.
- Hughes, S. A. & Thorne, K. S. 1998, *Phys. Rev. D*, 58, 122002.
- Isacson, R. A. 1968, *Phys. Rev.*, 166, 1272.
- Kuroda, K. et al. 2000, *Int. J. Mod. Phys. D*, 8, 557.
- Levin, Yu. 1998, *Phys. Rev. D*, 57, 659.
- Lindblom, L., Owen, B. J., & Morsink, S. M. 1998, *Phys. Rev. Lett.*, 80, 4843.
- Liu, Y. T. & Thorne, K. S. 2001, *Phys. Rev. D*, 62, 122002.

- Lück et al. 2000, in AIP Conf. Proc. 523, Proceedings of the 3rd Edoardo Amaldi Conference, ed. S. Meshkov (AIP: Melville), p. 119.
- Madau, P. & Rees, M. J. 2001, ApJ, 551, L27.
- Marion, F. 2000, in AIP Conf. Proc. 523, Proceedings of the 3rd Edoardo Amaldi Conference, ed. S. Meshkov (AIP: Melville), p. 110.
- McClelland, D. E. et al. 2001, in AIP Conf. Proc. 523, Proceedings of the 3rd Edoardo Amaldi Conference, ed. S. Meshkov (AIP: Melville), p. 140.
- New, K.C.B., Centrella, J.M., & Tohline, J.E. 2000, Phys. Rev. D, 62, 064019
- Owen, B. J., Lindblom, L., Cutler, C., Schutz, B. F., Vecchio, A., & Andersson, N. 1998, Phys. Rev. D, 58, 084020.
- Rampp, M., Müller, E., & Ruffert, M. 1998, A&A 332, 969.
- Santamore, D. H. & Levin, Yu. 2001, Phys. Rev. D, 64, 042006.
- Silk, J. 1983, MNRAS, 205, 705.
- Thorne, K. S. 1980, Rev. Mod. Phys., 52, 299.
- Thorne, K. S. 1987, in Three Hundred Years of Gravitation, eds. S. W. Hawking and W. Israel (Cambridge: Cambridge University Press), p. 330.
- Wang, L., Howell, D. A., Höflich, P., Wheeler, J. C. 2001, ApJ, 550, 1030.
- Wang, X., Tegmark, M., & Zaldarriaga, M. 2002, Phys. Rev. D, 65, 123001.
- Weiss, R. 1972, Quarterly Progress Report of the Research Laboratory of Electronics of MIT, 105, 54.